Geophysical Journal International

Geophys. J. Int. (2013) **193,** 1198–1215
Advance Access publication 2013 April 04

doi: 10.1093/gji/ggt065

An evaluation of the influence of the experimental cooling rate along with other thermomagnetic effects to explain anomalously low palaeointensities obtained for historic lavas of Mt Etna (Italy)

Lennart V. de Groot, Tom A. T. Mullender and Mark J. Dekkers

Paleomagnetic laboratory Fort Hoofddijk, Department of Earth Sciences, Utrecht University, Budapestlaan 17, 3584 *CD Utrecht, the Netherlands.*
E-mail: l.v.degroot@uu.nl

Accepted 2013 February 14. Received 2013 February 13; in original form 2012 March 18

SUMMARY

Methodological aspects in obtaining reliable absolute palaeointensity estimates have attracted renewed attention in recent years. Obtaining a reliable palaeointensity from lavas, however, still is notoriously difficult: in many cases lavas have been shown to be a non-ideal recorder of the palaeofield. Here we assess the influence of various thermomagnetic effects on the outcome of palaeointensity experiments on a suite of recent lavas from Mt Etna. Several palaeointensity studies have targeted recent flows of Mt Etna before; often palaeointensity underestimates were found. We apply both Thellier- and multispecimen-style palaeointensity experiments and obtain estimates generally 20–35 per cent below the expected reference value—in line with previous studies. We explored subtle chemical alteration, viscous magnetic behaviour and differences between the natural and laboratory cooling rates used during the palaeointensity experiments as possible causes for the observed underestimates of the palaeofield. For the latter, a furnace with controlled, programmable cooling rates was constructed. It can cool samples very slowly, with rates that are in the same order of magnitude as natural cooling rates typical of Mt Etna lava flows (∼10 K/day). Both viscous magnetic behaviour and differences in cooling rate appear to influence the outcome of the palaeointensity experiments. However, the magnitude of the changes observed is not sufficient to explain the observed underestimates. We, therefore, hypothesize that the observed underestimates may be primarily explained by transdomain processes occurring during the heating steps of the palaeointensity experiments.

Key words: Palaeointensity; Rock and mineral magnetism.

1 INTRODUCTION

The improvement of laboratory protocols has resulted in a renewed effort to obtain reliable absolute estimates of the intensity of the Earth's magnetic field from lavas at the time of their cooling. Several refinements of the classic Thellier–Thellier-style methods (Thellier & Thellier 1959) and new reliability tests have been proposed, such as partial thermoremanent magnetization (pTRM)-tail checks (Riisager & Riisager 2001), additivity checks (Krasa *et al.* 2003) and the 'IZZI' (in-field, zero-field, zero-field, in-field) protocol (Tauxe & Staudigel 2004; Yu *et al.* 2004; Yu & Tauxe 2005). Further, a number of new methods to obtain meaningful palaeointensities were put forward, including the microwave technique (Hill & Shaw 2000), a reassessment of the Wilson method (Muxworthy 2010) and the multispecimen approach (MSP; Dekkers & Böhnel 2006; Fabian & Leonhardt 2010). Seeking natural material with the optimal grain size range for palaeointensity determinations [ideally grains should be single-domain (SD)] was the topic of yet another set of studies. The potential of magnetic inclusions in single crystals was explored by Cottrell & Tarduno (1999), whereas volcanic glasses with inherently very fine-grained material were studied by Tauxe *et al.* (1995), Juarez *et al.* (1998), Bowles (2005), Leonhardt *et al.* (2006) and Ferk *et al.* (2010).

Acquiring a reliable palaeointensity from recent lavas of Mt Etna (Sicily, Italy) has been shown to be notoriously difficult (Tanguy 1975; Haag *et al.* 1995; Hill & Shaw 1999; Calvo *et al.* 2002; Biggin *et al.* 2007a,b). These studies used both thermal and microwave Thellier-style palaeointensity techniques and generally find inconsistent results. Here, we subject samples from fifteen independent locations from five different flows dated between 1923 and 2002 of Mt Etna to both the Aitken Thellier protocol (Aitken *et al.* 1988) and the recently proposed MSP (Dekkers & Böhnel 2006; Fabian & Leonhardt 2010). Four sites included in this study were discussed in de Groot *et al.* (2012) and yielded unexplained underestimates of the palaeofield. All the other sites also yield underestimates of the palaeofield, for both Thellier- and MSP-style experiments. This is in line with previous findings by Hill & Shaw (1999), Calvo *et al.* (2002) and Biggin *et al.* (2007a).

We explore various potential causes of these underestimates: subtle chemical alteration induced by laboratory heating, viscous

magnetic effects and differences between natural and laboratory cooling rates. To assess the latter, a designated furnace with controlled cooling rates was constructed. Very slow cooling is now possible—at a rate of only 10.8°C day^{-1}, closely mimicking natural cooling. The relatively thin lava flows discussed here were modelled to have cooled naturally with a rate similar to within an order of magnitude of our experimental cooling rate (Harris & Rowland 2001).

2 GEOLOGICAL SETTING AND EARLIER PALAEOINTENSITY STUDIES

Our collection of historic Mt Etna eruptions comprises 15 sites from the 1923, 1971, 1979, 1983 and 2002 flows. Typically a site consists of a horizontal 'line' of 8-12 closely spaced drill cores to ensure among-sample homogeneity as much as is realistically possible. At some sites multiple 'lines' of samples were drilled at different distances from the top of the flow. Table 1 provides the specifications of all sites: GPS locations, international geomagnetic reference field (IGRF) reference values and location of the samples within the flow; Fig. 1 shows their locations on a map.

We sampled the 1923 flow at two locations: site 23-1 at the southernmost and highest paved road crossing the flow, and site 23-2 along the lower through-road between Linguaglossa and Randazzo. Three sites in the 1971 flow were sampled west of the village of Fornazzo. Site 71-2 is the eastern-most 1971-site, sites 71-1 and 71-3 are close together approximately one km further uphill. The 1979 flow is close to the 1971 flow, which it partly overlays. The 1979 flow was sampled at one location: 79-1 was taken along the '*Via Mareneve*', close to Fornazzo. The lava of the 1983 eruption is to the south of the summit of Mt Etna. There are several good road-cut outcrops along the through-road from the city of Nicolosi towards the summit access. The 1983 flow was therefore sampled at 6 different sites. Sites 83-1, 83-2 and 83-3 were taken close to each other: sites 83-2 and 83-3 are *in situ* in a road cut. Site 83-1 was taken from a large block, broken from the same road cut. This block measures *ca.* 1.8 m × 1.8 m × 0.7 m and its original position in the flow could be identified unambiguously. Five lines were drilled at distinct distances from the top of the flow: Site 83-1A was drilled 15 cm below the top and 165 cm from the bottom; site 83-1B at 45 cm below the top and 135 cm from the bottom; site 83-1C at 90 cm from the top and 90 cm from the bottom; site 83-1D at 133 cm from the top and 47 cm from the bottom; and site 83-1E at 168 cm below the top and 12 cm from the bottom of the flow. Because of their different heights in the flow these sites have experienced different cooling rates. The 1983 flow was further sampled at three other locations: sites 83-4 and 83-5 were taken close to each other ∼3.5 km further uphill along the road. Site 83-6 was drilled another 3 km further uphill along the road. The most recent flow included in this study was the flow of the 2002 eruption sampled a few kilometres north of the 1971 flow. The 2002 flow was sampled at three locations: Sites 02–1 and 02–3 were sampled along the road between Fornazzo and Linguaglossa; site 02–2 approximately 1 km higher along a secondary road leading to a small ski resort.

Except for the sites from the 2002-flow, Hill & Shaw (1999), Calvo *et al.* (2002) and Biggin *et al.* (2007a) reported on palaeointensities of the flows in this study. Hill & Shaw (1999) primarily use a version of the microwave Thellier method to obtain their palaeointensity estimates, whereas Calvo *et al.* (2002) and Biggin *et al.* (2007a) use several versions of thermal Thellier-style protocols. In these three studies the sites are categorized into rock-magnetic groups. In the Hill & Shaw (1999) study samples with 'pseudosingle-domain (PSD) to SD characteristics' (their group A) yielded palaeointensities close to the expected IGRF values. Samples with 'PSD to multidomain (MD)' and MD characteristics (groups B and C respectively) gave underestimates of the palaeofield. Calvo *et al.* (2002) categorized their sites based on the behaviour of the magnetic susceptibility with temperature. Samples with a single dominant high Curie temperature (>400°C; termed type H) generally yield palaeointensity overestimates; samples with multiple Curie temperatures (type C) provide similar results. Their type M samples—with a high dominant Curie temperature during heating, but with a much lower dominant Curie temperature during cooling—generally yield underestimates of the palaeofield. Biggin *et al.* (2007a) report dependence between the thermal 'hardness' of a sample and the outcome of the Thellier result. Their 'hard-type' samples (samples in which less than 60 per cent of their natural remanent magnetization (NRM) is demagnetized at 350°C) tend to yield approximately correct palaeointensity values or overestimates. Their 'soft-type' samples (samples in which more than 50 per cent of their starting NRM is demagnetized at 350°C) generally yield approximately correct palaeointensity estimates or underestimates. Rock-magnetic groups very similar to those distinguished by Calvo *et al.* (2002) and Biggin *et al.* (2007a) will be used in this study as well. The mineralogical and petrographical properties are described in depth in those studies.

3 METHODS

3.1 Palaeomagnetic and rock-magnetic analyses

To identify the best temperature or range of temperatures for the palaeointensity experiments, samples from all sites were subjected to various (thermal) rock-magnetic analyses. The NRM decay curves and palaeomagnetic directions were assessed by classical stepwise progressive demagnetization experiments, both thermally and by alternating fields. All thermal experiments were done using a 2G DC-SQUID magnetometer and an ASC TD48-SC thermal demagnetizer. Typically, samples were demagnetized in 14 steps to less than 5 per cent of their starting NRM at 580°C. The alternating field demagnetization experiments were done using a robotized 2G DC-SQUID magnetometer. Typically, samples were demagnetized in 18 steps to less than 10 per cent of their starting NRM at 100 mT. To check whether the sampled flows are *in situ*, the palaeomagnetic directions of a number of samples were obtained using oriented cores.

Chemical alteration in the samples should be avoided during the palaeointensity experiments. Therefore, samples from all sites were subjected to both high- and low-field thermomagnetic analyses. The magnetic susceptibility was measured as a function of temperature on an AGICO KLY-3S susceptometer with a CS-3 furnace attachment (in air). The temperature was cycled to progressively higher temperatures to test the reversibility of the signal. A non-reversible signal indicates (chemical) alteration in the sample. The behaviour of the high-field magnetization of the sample as function of temperature was assessed with a modified horizontal translation Curie balance (Mullender *et al.* 1993). Again, the temperature was increased in cycles up to 700°C and non-reversible behaviour indicates (chemical) alteration. Both analyses were done in air.

Based on the susceptibility versus temperature diagrams, most of the sites can be categorized in the groups as introduced by Calvo *et al.* (2002) and, with minor changes, also used by Biggin *et al.* (2007a). Here we use the following three types. (1) 'Type L': with

Table 1. Site locations and reference data. From left to right: site-codes (first two digits indicate year of eruption, e.g. 23 = 1923, 02 = 2002); line-code; distance to the top and bottom of the flow (massive part); thickness of overlying scoria; dominant Curie and alteration temperatures; assigned rock-magnetic groups (based on the susceptibility versus temperature diagrams if available; an "*" indicates a rock-magnetic group assigned based on the magnetization versus temperature diagram); exact locations with GPS error; and international geomagnetic reference field (IGRF) reference data (dec = declination; inc = inclination; int = intensity) for sites presented in this study. Selected rock-magnetic data of sites indicated with '°' were previously included in de Groot *et al.* (2012).

Site	Line	Distance to top (m)	Distance to bottom	Scoria thickness (m)	Curie T (°C)	Alteration T(°C)	Rockmagnetic group	Latitude (N)	Longitude (E)	GPS error (m)	IGRF (dec)	IGRF (inc)	IGRF (int; uT)
	A	0.25	1.35		–	–	–						
23-1	B	0.93	0.68	0.5	240	>320	L	37° 50′ 42.27′	15° 4′ 50.8′	6	−5° 42′	52° 46′	42.2
	C	1.50	0.20		–	–	–						
23-2°	–	0.95	0.65	–	520	>320	C	37° 51′ 13.51′	15° 6′ 51.19′	4	−5° 42′	52° 46′	42.2
71-1	–	0.50	1.20	1.5	260	>320	L	37° 45′ 7.13′	15° 5′ 11.4′	9	−0° 39′	53° 40′	43.9
	A	0.33	1.22		420	> 320	C						
71-2	B	0.80	0.72	0.3	220	>400*	L*	37° 44′ 53.63′	15° 5′ 57.36′	7	−0° 39′	53° 40′	43.9
	C	1.25	0.09		–	–	–						
	A	0.95	0.10		–	–	–						
71-3°	B	0.50	0.55	1.0	220	>300	L	37° 45′11′	15° 5′12.59′	4	−0° 39′	53° 40′	43.9
	C	0.15	0.55										
	A	0.15	1.40		450	>400*	C*						
79-1°	B	0.75	0.75	0	260	>280	L	37° 44′ 26.77′	15° 5′ 58.1′	5	0° 20′	53° 10′	44.1
	C	1.40	0.10										
	A	0.15	1.65		550	>350*	H						
	B	0.45	1.35		560	>350*	H						
83-1	C	0.90	0.90	–	550	>350*	H	37° 40′ 32.73′	14° 58′ 56.68′	5	−0° 23′	52° 57′	44.2
	D	1.33	0.47		540	>350*	H						
	E	1.68	0.12		550	>350*	H						
83-2	–	–	–	–	550	>350*	H*	± 5m North of 83-1 (*in situ*)			−0° 23′	52° 57′	44.2
83-3	7.0	–	–	–	460	>350*	H	37° 40′ 32.96′	14° 58′ 55.62′	5	−0° 23′	52° 57′	44.2
	A	1.60	0.15		440	>380	C						
83-4°	B	1.10	0.95	2.5–3.0	260	>350	L*	37° 41′42.37′	14° 59′28.15′	6	−0° 23′	52° 57′	44.2
	C	0.28	1.20		480	>350*	C*						
83-5	–	0.26	0.25	2.5–3.0	200	>350*	L*	± 20m East of 83-4			−0° 23′	52° 57′	44.2
83-6	–	0.90	–	1.5	375	>390	C	37° 41′ 17′	14° 59′ 13.86′	5	−0° 23′	52° 57′	44.2
	A	0.30	1.60		430	>320	C						
02-1	B	0.70	0.65	0.5	500	>320	H	37° 47′ 44.3′	15° 3′ 43.26′	8	1° 47′	53° 26′	44.7
	C	1.80	0.20		470	>320	H						
02-2	–	1.30	–	1.0	470	>330	H	37° 47′41.23′	15° 3′24.37′	4	1° 47′	53° 26′	44.7
02-3	–	0.90	–	1.0	560	>400*	H*	37° 47′49.75′	15° 3′ 52.3′	4	1° 47′	53° 26′	44.7

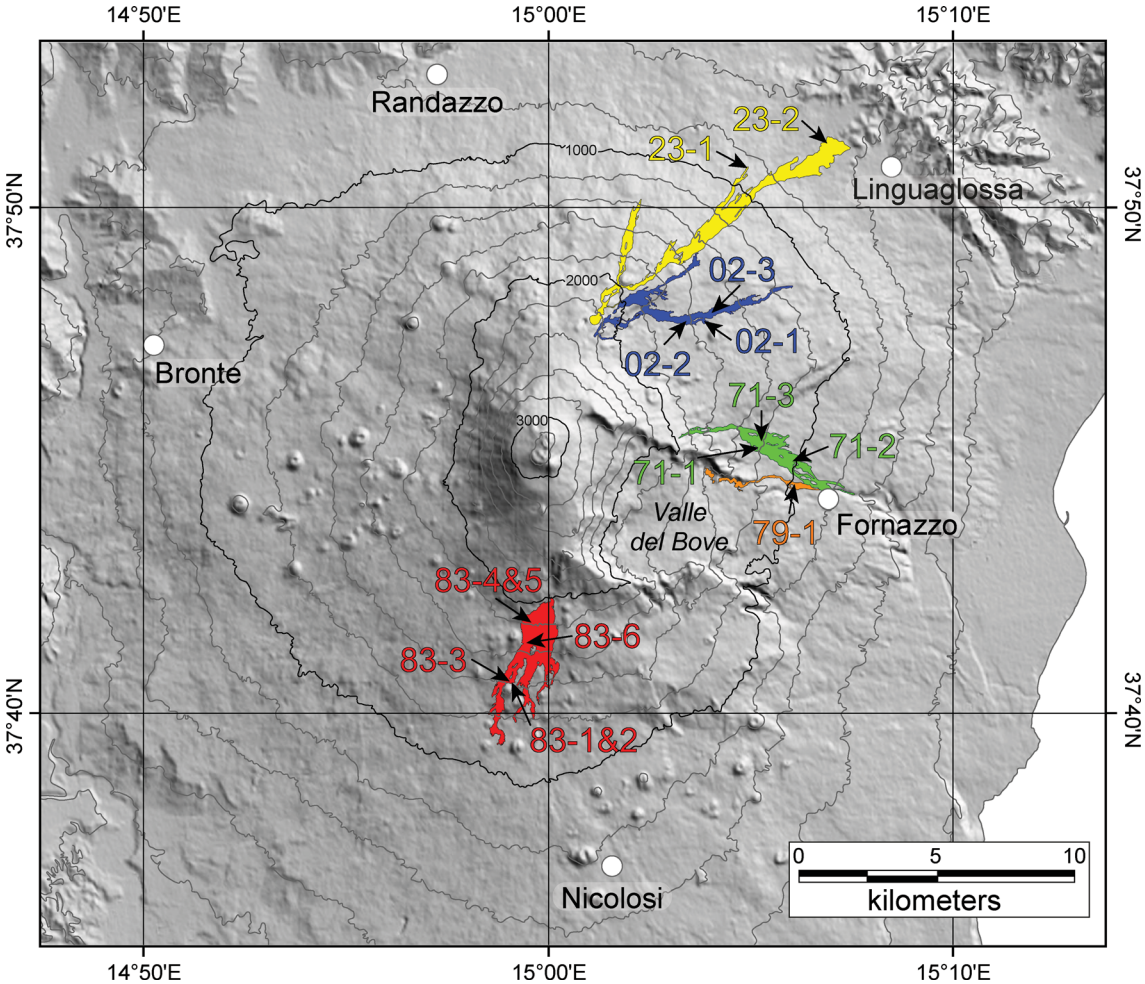

Figure 1. Digital elevation model of the Etna region with the sampling locations of this study. The sampled flows are indicated as follows: the 1923-flow in yellow, the 1971-flow in blue, the 1979-flow in orange, the 1983-flow in red and the 2002-flow in blue. The contour interval is 200 m. See Table 1 for GPS locations and reference data of the sites. DEM-map courtesy of INGV, Catania.

a distinct low Curie temperature, losing more than 50 per cent of its susceptibility below 250°C. (2) 'Type H': with a distinct high Curie temperature, with increasing susceptibility until at least 350°C. (3) 'Type C', with either a broad Curie spectrum, an indication of a heterogeneous titanomagnetite composition (Dunlop & Özdemir 1997), or multiple Curie temperatures, indicating a combination of the H- and L-type compositions.

To assess the magnetic grain size distribution in our data set, a Day plot (Day *et al.* 1977) is used. The parameters needed to assemble a Day plot—saturation magnetization (M_s), remanent saturation magnetization (M_{rs}), coercive force (B_c) and remanent coercive force (B_{cr})—were measured on a Princeton instruments alternating gradient force magnetometer, PMC Model 2900. The samples were magnetically saturated using a field of at least 1 T and the field increment was set between 4 and 7.5 mT to obtain a suitable resolution for each sample.

3.2 Thellier-style palaeointensity experiments

Various refinements have been made to the classical Thellier palaeointensity protocol since it was introduced by Thellier & Thellier (1959), particularly concerning the order of the remagnetization and demagnetization steps. In the protocol proposed by Coe (1967) each demagnetization step is followed by a pTRM remagnetization step at the same temperature. Kono & Ueno (1977) used only one heating per temperature, which makes it necessary to align the samples with their NRM to the applied field during the experiment. In the Aitken protocol (Aitken *et al.* 1988; Valet *et al.* 1998; Biggin & Böhnel 2003) the order of the demagnetization and remagnetization steps at each temperature is reversed: the pTRM step precedes the demagnetization step at each temperature. More recently an alternating protocol was proposed to reveal the presence of magnetic memory effects and minimize their impact on the interpretation of the Thellier-style results, termed 'IZZI' (Tauxe & Staudigel 2004; Yu *et al.* 2004; Yu & Tauxe 2005). Here, we use the Aitken protocol in the Thellier-style experiments. This makes the results of the Thellier-style palaeointensity experiments more analogous to the 'multispecimen-style' (MSP) palaeointensity experiments (described below), in which a pTRM is imparted on every sample only once.

As is shown in the results section the preliminary rock-magnetic experiments indicate thermochemical alteration beyond 350°C. Therefore, the Thellier-style experiments were terminated after reaching 340°C. In total eight temperature steps were used: 100,

130, 150, 180, 210, 240, 280 and 340°C. To test for alteration in the samples during the experiment, in-field steps at the preceding temperature were repeated. These pTRM checks (Coe 1967) were applied at all temperature steps except 180, 240 and 340°C.

For the data interpretation the program Thellier-tool 4.22 (Leonhardt *et al.* 2004) was used providing various reliability parameters of the Thellier experiments. Here, we include the number of temperature steps included in the linear fit (N), the angle between the origin-anchored and floating line fits in the Zijderveld plot (α); the fraction (f), gap (g) and quality (q) factors (Coe 1978); the ratio of the standard error of the slope of the line fit and the slope (β); and the difference ratio DRAT (Selkin & Tauxe 2000). All accepted Thellier plots are based on at least 6 data points ($N \geq 6$) and yield a gap factor above 0.70 ($g \geq 0.70$). Because it is very important that the samples do not alter during a Thellier-style experiment—that would invalidate the premise that the pTRMs should be imparted under the same (chemical and magnetic) conditions as the NRM was acquired in—we chose to terminate the Thellier-style experiments at 340°C, just below the alteration temperature indicated by the preliminary rock-magnetic experiments (350°C). Therefore, some specimens unblocked only a small portion of the NRM, leading to relatively small f-values and low q-values. Based on the above parameters the Thellier results are grouped in the following categories:

- 'A': $f \geq 0.30$, $\beta \leq 0.15$, $q \geq 3$ and DRAT $\leq$ 15 per cent.
- 'B': $f \geq 0.30$, $\beta \leq 0.20$, $q \geq 2$ and DRAT $\leq$ 20 per cent.
- 'C': not meeting the criteria for A or B.
- 'H': $f < 0.30$.
- '2sl': distinct two-slope behaviour in the Arai plot.
- 'F': not interpretable.

For mere comparison with the IGRF field values and to enable comparison to the MSP-style results in this study more Thellier results are interpreted than one would normally be inclined to (category B and certainly categories C, H and 2sl would not be considered to be meaningful).

3.3 MSP palaeointensity experiments

3.3.1 Classic MSP experiment

Besides the Thellier technique, the differential parallel multispecimen palaeointensity technique (MSP; Dekkers & Böhnel 2006) was applied to the sites included in this study. In the MSP technique several sister specimens are used and heated to the same temperature to rule out magnetic history effects that complicate MD palaeointensity experiments. This temperature is referred to as 'set temperature'; it is obviously lower than the temperature range at which thermochemical alteration is occurring. During heating and cooling the sister specimens have their NRM aligned with the laboratory DC field. For each specimen the difference between the imparted pTRM as function of laboratory field intensity and the NRM is divided by the NRM. By plotting this ratio as a function of the applied DC field, the x-axis intercept—-the laboratory field for which the total magnetization of a specimen does not change after imparting a pTRM—can be determined. This is argued to be equal to the ancient natural Earth's magnetic field in which the specimen originally cooled. The confidence interval of the MSP experiments is obtained by determining the x-axis intercepts of the one-standard-deviation interval around the fit. Furthermore, the number of samples (n), the slope of the fit (a), the y-axis intercept (b) and the coefficient of determination (r^2) of the linear fit are given. If data points fall outside the one-standard-deviation error envelope, the linear fit and its one-standard-deviation error envelope are recalculated omitting these points.

3.3.2 Tail-corrected MSP experiment

Following the phenomenological theory by Fabian & Leonhardt (2010) the MSP protocol also suffers to some degree from magnetic tail and domain state effects that occur during imparting pTRMs in non-SD particles. These effects cause the original MSP protocol to systematically overestimate the palaeointensities. Fabian & Leonhardt (2010) propose refinements to the MSP method to correct for these effects. Three extra steps are added to the original single-step MSP protocol [step 2: heating and cooling in an antiparallel DC field; step 3: heating in zero field, cooling in parallel DC field; and step 4: heating and cooling in parallel field (a repeat of step 1)] to quantify domain state and tail effects. This extended protocol is further referred to as 'MSP-DSC' and, following the nomenclature of Fabian & Leonhardt (2010), the original single-step MSP protocol is further referred to as 'MSP-DB'. The α-parameter in the MSP-DSC analysis was set to 0.5, as suggested by Fabian & Leonhardt (2010).

3.3.3 Testing for subtle chemical alteration

As shown in the results section, both the Thellier and the MSP methods generally yield underestimates of the palaeofield for all sites included in this study. To test whether atmospheric oxygen (the samples are heated in air) might be the cause of the unexpected results of the MSP-DB experiments, the MSP-DB experiments for sites 23-1C, 71-2B and 83-4B were repeated using sister specimens while heating and cooling the samples in an argon atmosphere. The controlled atmosphere insert of the ASC TD48-SC oven was thoroughly flushed with argon (technical grade) after inserting the samples; it was continuously flushed (with a low rate) during heating and cooling of the samples to remove any oxygen or other gasses escaping from the samples during the thermal cycle. This experiment is referred to as the 'MSP-DB in argon experiment'.

The experiments in an argon atmosphere are not entirely conclusive concerning the interpretation of chemical alteration, since the internal oxygen fugacity within the samples might be an important issue. Further, unmixing of titanomagnetite or titanomaghemite into a magnetite-rich and a ilmenite-rich end-member might still occur at temperatures near those used in the palaeointensity experiments independent of the ambient atmosphere in the furnace (i.e. air or argon). Therefore samples from sites 23-1A, 79-1A and 83-4C were given a full laboratory TRM at 600°C in an argon atmosphere forcing the aforementioned processes to occur if the samples are prone to show them. Half of these samples were used for a MSP-DB experiment in air; the other half was subjected to a MSP-DB experiment in argon. The full TRM is imparted with a typical laboratory cooling rate (15–20°C min^{-1}). Due to the heat capacity and the thermal insulation of the controlled atmosphere insert, the cooling rate of the samples during the full TRM acquisition cannot be exactly the same as the cooling rate in the palaeointensity experiments (that typically involve imparting a pTRM at 250°C). However, they can be considered the same to within an order of magnitude. This experiment will be referred to as the 'full TRM MSP-DB experiment'.

3.3.4 Testing for viscous behaviour

To test for viscous behaviour of the imparted pTRMs, the samples from sites 71-2B and 83-4B that underwent a MSP-DB experiment

were measured again after storing the samples randomly orientated in the Earth's magnetic field for two weeks (step II; note that step I is the first MSP-DB experiment). This second step, although not equal to a proper determination of the viscosity index (Prévot *et al.* 1981), is a first-order indicator of magnetization changes on short (laboratory-) timescales that may occur in the samples. After this step II, the MSP-DB experiment was repeated: the same samples were heated again in the same orientation in the same DC field during the thermal cycle to the same set temperature as in the first experiment. Then the samples were measured for a third time (step III). As a last step the MSP-DB experiment was repeated again, without storing the samples in between the experiments, for a third time (step IV). This protocol will be further referred to as 'random time regime'.

To further test for the influence of changes on laboratory-timescales, the MSP-DB experiments were repeated three times on samples from sites 71-3C and 83-4A. In contrast to the 'random time regime' experiment described above, now the timing of the different experiment stages—heating, cooling, taking samples out of the oven, measuring and putting the samples in the oven again—was done in a strict time regime. Both the duration of the different stages and the time between them was clocked and kept equal to within a minute. This protocol will be further referred to as 'strict time regime'.

3.3.5 Cooling-rate effects

Cooling-rate effects in acquiring TRMs and pTRMs have been studied for a few decades with mixed results. For SD grains both theory and experiments show that the TRM intensity increases for slower cooling rates (Dodson & McClelland-Brown 1980; Halgedahl *et al.* 1980; Walton & Williams 1988 and more recently by Leonhardt *et al.* 2006; Ferk *et al.* 2010). For MD grains the opposite trend is sometimes observed: a slower cooling rate yields lower TRMs (McClelland-Brown 1984; Perrin 1998), although the theory for these grain sizes is poorly understood. Very recently, Yu (2011) showed that the effect of the cooling rate on the outcome of the palaeointensity experiment is insignificant for the PSD range. He experimentally tested laboratory cooling rates of ∼40 and ∼3 K min^{-1}.

To assess the influence of the (laboratory-) cooling rate on the acquired pTRM—and therefore the result of the palaeointensity protocol—a dedicated cooling-rate furnace was built which is capable of cooling at a rate similar to natural cooling rates for lavas. This furnace is in essence a thermal demagnetizer with improved thermal insulation to increase the thermal stability. Several thermocouples inside the system monitor and control the temperature. The temperature-time trajectory is computer-controlled and can be programmed to follow specific pre-defined profiles. We describe it briefly below because it can cool as slow as $\sim 2 \times 10^{-3}$ K min^{-1}, a rate at least an order of magnitude slower than other, more conventional, slow-cooling thermal demagnetizers.

The furnace has an outer diameter of 150 mm and is positioned inside a triple mumetal tube (1400 mm long, diameters 230, 260 and 290 mm). As classically applied in thermal demagnetizers, the furnace consists of three heating zones: one central zone in which the samples are placed and two outer zones for thermal stability. All three are independently controlled with 'type N' thermocouples for extremely good temperature stability. Each heating zone has a separate heater ribbon of NiChrome V which is wound in a bifilar fashion on an alumina tube of 76 mm inside diameter. The three controllers can be set with 0.1 Kelvin steps through RS485 communication with a PC under Labview control. A layer of high-quality thermal insulation material encloses an inner quartz tube of 52 mm diameter. Inside this quartz tube a maximum of ten standard-size specimens are mounted and thermally coupled to the high thermal mass of a solid brass sample holder, together with a fourth type N thermocouple to monitor specimen temperature with time. The thermally stable sample space inside this quartz tube is 400 mm long. It is equipped with a linearized DC field coil (for in-field experiments, capable of reaching 250 μT), linear to within 0.5 per cent. The effective high thermal mass combined with the high thermal resistance functions as a first-order low-pass filter with a time constant of >7000 s. The Labview program uses a first-order noise shaping technique to avoid a 'stair-like' temperature profile with steps of 0.1 K. Temperature control data sets show a non-correlated deviation of maximum 0.2 K (peak) from set point, over periods of 5–15 min. Using the thermal time constant of 7000 s this translates to a slowest possible ramp rate of $\sim 3 \times 10^{-5}$ K s^{-1} ($\sim 1.8 \times 10^{-3}$ K min^{-1}). The furnace is capable of reaching temperatures up to 600°C.

In our experiments an average linear cooling rate of 1.25×10^{-4} K s^{-1} (or 10.8 K day^{-1}) was used. Effectively, the cooling rate varied randomly between 9.5×10^{-5} K s^{-1} and 1.55×10^{-4} K s^{-1} on timescales in the order of tens of seconds to a few minutes. For comparison, the cooling rate of the ASC TD48-SC thermal demagnetizer is typically 2.5–3.0 $\times 10^{-1}$ K s^{-1} for the temperature range used in our experiments (250°C and lower), but this cooling rate becomes non-linear for temperatures closer to room temperature. The cooling rate of the furnace described above is thus approximately three orders of magnitude slower than a typical thermal demagnetizer.

Four lines of site 83-1 (B-E) were selected for the cooling-rate experiments. These samples, taken at different depths in the flow, acquired their NRM with different cooling rates: the samples closer to the top are expected to have cooled faster than the samples towards the middle and bottom of the cooling unit. The lowermost parts of the lava also cool from below, although this cooling is less efficient than cooling from the top.

3.4 Intensity error fraction

To assess the accuracy of the palaeointensity protocols in recovering the expected IGRF values, the intensity error fraction (IEF) is used (Biggin *et al.* 2007a). The IEF is calculated by dividing the result of the palaeointensity experiment by the expected IGRF value for that site and expressed as a percentage.

4 RESULTS

4.1 Rock-magnetic analysis

The sites in this study can be categorized in the three groups with the different rock-magnetic behaviour outlined before (Table 1). Typical thermal decay curves (Fig. 2a) show higher unblocking temperatures for rock-magnetic group H, whereas rock-magnetic groups C and L are reasonably identical. The coercivity behaviour of groups H and C is more alike; their AF decay curves are within each other's one-standard-deviation error envelope (Fig. 2b). Group L shows a very soft behaviour loosing approximately 75 per cent of its NRM at 25 mT. Groups H and C are harder; they lose ∼50 per cent of their NRM at that alternating field level. In the Day plot (Fig. 2c) the difference between the rock-magnetic groups

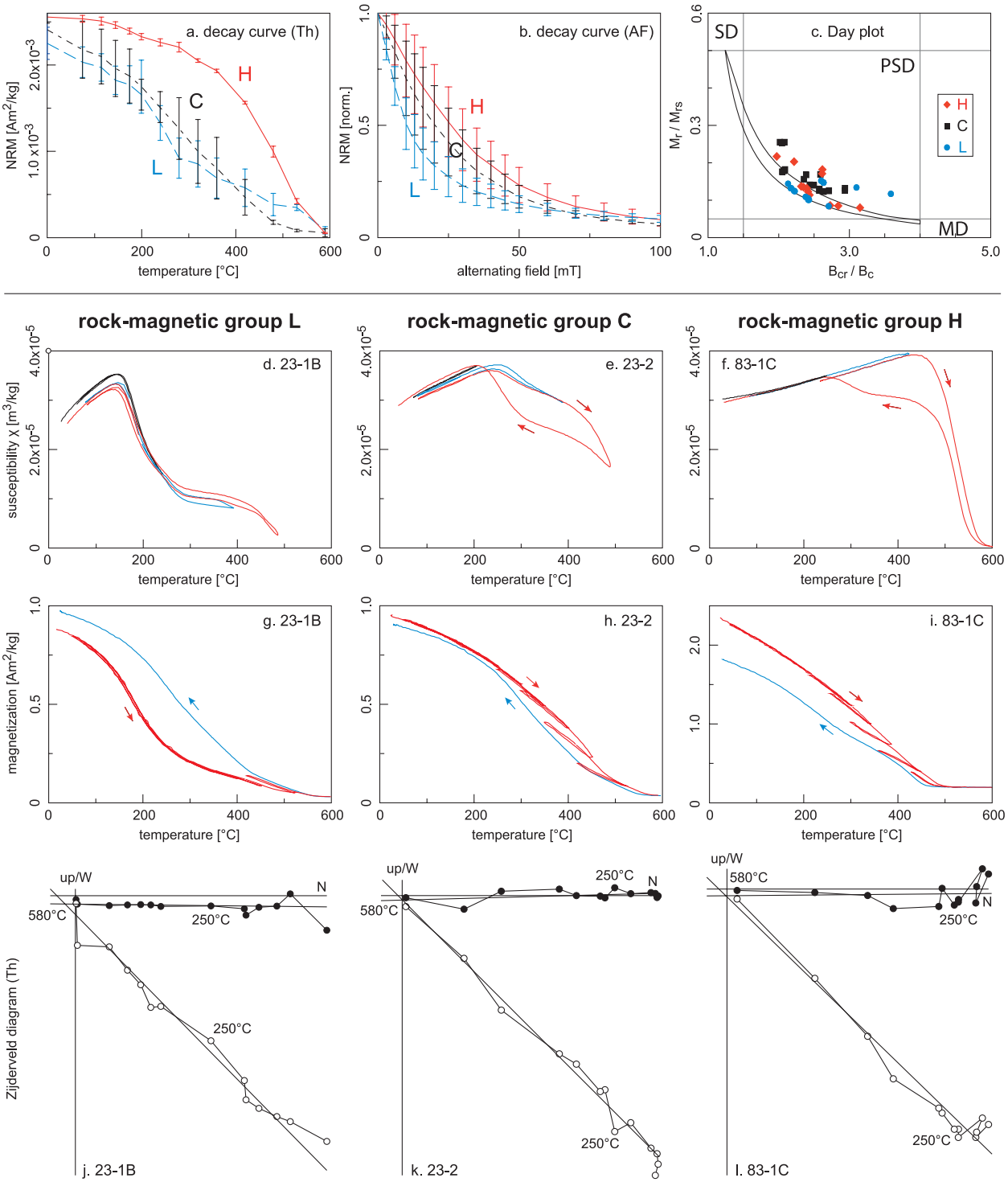

Figure 2. Rock-magnetic analyses. Based on rock-magnetic properties, the sites are categorized in three groups: H, C and L. Typical specific NRM decay curves for these groups are shown in panel (a) (thermal, Th) and panel (b) (coercivity, AF). Group H is depicted as solid red line, group C as interchanging short and long black dashes and group L as long blue dashes. The thermal decay curves are averaged after normalizing the intensities to the mass of the samples, the error bars indicate one standard deviation above and below the average. The AF decay curves are averaged after normalizing the NRM to 1, again the error bars indicate one standard deviation above and below the average. The Day plot for the sites is given in panel (c): group H is depicted as red diamonds, group C as black squares and group L as blue dots. The theoretical SD+MD mixing curves (Dunlop 2002) are indicated as curved black lines, the upper line was calculated using the coarse-grained end-member data, the lower line using the fine-grained end-member data of Parry (1965) and Day *et al.* (1977). Panels (d–f) show typical susceptibility versus temperature plots for rock-magnetic groups L, C and H respectively; temperature cycles to increasingly higher temperatures are indicated with black, blue and red curves. Panels (g–i) show typical magnetization versus temperature plots for the same sites as used for panels (d–f); the heating curve (with intermittent cooling segments) is depicted in red, the final cooling curve in blue. Zijderveld diagrams of thermal demagnetization experiments for these sites are shown in panels (j–l), respectively; the samples used for this analysis were taken unoriented, for ease of comparison the average declination and inclination are forced to be approximately 0 and 45°, respectively.

is less distinct. Generally group L yields the lowest M_{rs}/M_s ratios, group C the highest and group H is in between. In terms of B_{cr}/B_c ratios, the three groups do not show different behaviour. All data points plot within the PSD range and slightly above the theoretical SD + MD mixing curve for the fine-grained end-member of Day *et al.* (1977), Parry (1965) and Dunlop (2002). Note that the hysteresis loop analysis, on which the Day plot is based, is a high-field experiment on a bulk sample. Hysteresis loop measurements tend to over-represent larger particles because they represent most mass or volume. The obtained Day-parameters might be slightly biased to the bigger grains. Information on the size distribution of magnetic grains in the sample cannot be readily obtained from this diagram. Unimodal particle-size distributions of trace constituents are often approximately lognormal. The (remanent) coercive force would be approximately equivalent to the geometric mean of the coercivity distribution.

The susceptibility versus temperature diagrams (Figs 2d–f) are the main discriminator between the rock-magnetic groups, so their variation within the groups is minimal. For rock-magnetic group H, the Curie temperature is well defined by a steep decrease of susceptibility around 500°C, indicating a single, or at least dominant, magnetite-like magnetic carrier. Group L shows a much lower Curie temperature at ∼200°C and a second one at ∼450°C. Arguably, a third Curie temperature can be identified at ∼250°C. This indicates that there are more minerals contributing to the net magnetic moment of the sample. Rock-magnetic group C reveals an even broader spectrum of Curie temperatures: between 250 and 500°C the susceptibility decreases gradually, indicating a wide range of titanomagnetite compositions (possibly a nearly continuous solid solution of titanomagnetites with various titanium-iron ratios).

The magnetization versus temperature diagrams also reveal the Curie and alteration temperatures, but often in a less distinct manner. The magnetization versus temperature diagram of group L (Fig. 2g) shows a low Curie temperature and an increase in both magnetization and Curie temperature after heating to 600°C; group C (Fig. 2h) reveals a very broad Curie temperature spectrum, with not that much alteration, even after heating to 600°C. The behaviour of group H (Fig. 2i) is broadly opposite to that of group L: a high Curie temperature—but not as distinct as in the susceptibility versus temperature plots—and a lower magnetization and Curie temperature during cooling from 600°C. It should be realized that (saturation) magnetization versus temperature behaviour is a material property: it reflects the chemical composition of the magnetic mineral suite. In susceptibility versus temperature experiments structural changes in a sample may also be determined; subtly irreversibly changing susceptibility behaviour hints at incipient thermochemical alteration. Note that susceptibility versus temperature runs inherently focus on magnetite because of its very high low-field susceptibility compared to other magnetic minerals. For the rock-magnetic group L, the Curie temperatures are generally well defined in both types of analysis, implying a reasonably homogeneous grain size and composition distribution of the magnetic carriers. For groups C and H the magnetization decreases roughly linearly between room temperature and 500°C. For group C this agrees with the observed compositionally variable mineral content as inferred from the susceptibility versus temperature analysis. For group H, however, the susceptibility versus temperature analysis indicates a reasonably well-defined single carrier. It is an example of the dominance of magnetite-like material in this type of measurement. The magnetization temperature behaviour indicates Ti-poor titanomagnetite that alters on heating above ∼400°C.

The directional data for all sites is in good agreement with the expected IGRF values, implying that the samples were taken *in situ*, no movement of lava blocks took place after cooling. This also implies that potentially present local field anomalies (Baag *et al.* 1995; Valet & Soler 1999) have insignificant influence on the directional behaviour of the samples. No or very small overprints are present in the samples; they are removed by <5 mT AF or a heating step <100°C.

Based on the rock-magnetic analyses above, the most suitable set temperature for the MSP experiments and the most suitable temperature range for the Thellier style experiments are determined (Table 2). A sufficiently large portion of the NRM should be unblocked during the palaeointensity experiments, whereas alteration should be avoided. In general, no signs of alteration occur up to 320°C; at that temperature more than 50 per cent of the NRM unblocks for rock-magnetic groups C and L, and 10–15 per cent of the NRM unblocks for group H.

4.2 Thellier results

The results of the Thellier experiments vary in quality (Table 2, Fig. 3). Of the 31 sites included in this study, five sites (16 per cent) yield results that meet the criteria for category A; seven other sites (23 per cent) meet the criteria for category B. Three sites show distinct two-slope behaviour (10 per cent); two sites (6 per cent) demagnetize less than 30 per cent of their NRM before they reach their alteration temperature and nine sites (29 per cent) yield results that are not interpretable. The remaining five sites do yield a linear fit, but do not meet any of the selection criteria (category C). All sites appear to yield underestimates of the palaeofield with the exception of site 23-2 (45.9 μT, an IEF of 8.7 per cent). For category A sites the palaeointensity varies between 24.1 and 37.7 μT (Table 2), corresponding to underestimates of the expected IGRF values between 14.1 and 45.1 per cent. If category B sites are also considered, the obtained palaeointensities vary between 24.1 and 42.8 μT: yielding IEFs between −45.1 and −4.2 per cent.

Sites belonging to rock-magnetic group H were largely unsuccessful in Thellier experiments—seven out of nine 'failures' are from group H. The sites from group H that do yield technically reliable palaeointensity estimates give values closer to the expected IGRF values than sites from the other rock-magnetic groups. The results are, however, still considerable underestimates: an average IEF of −23 per cent (four sites). All category A results and three out of seven category B results are from sites belonging to rock-magnetic group L with an average IEF of −37 per cent. The average IEFs for rock-magnetic groups L and C are statistically indistinguishable: −37 per cent (seven sites) and −39 per cent (six sites), respectively. All obtained palaeointensities underestimate the palaeofield well beyond the range anticipated to result from possible local field anomalies (Baag *et al.* 1995; Valet & Soler 1999).

4.3 MSP results

4.3.1 Classic MSP experiment

The MSP-DB experiments all yield underestimates of the palaeofield (Table 2, Fig. 4). Generally, the results are technically correct and consistent among sites from the same flows. The obtained palaeointensities range between 24.4 and 35.3 μT, implying IEFs between −44.8 and −19.6 per cent. The width of the one-standard-deviation error envelope around the fit depends on both the number

Table 2. Palaeointensity results. From left to right: site and rock-magnetic group (G); Thellier parameters and results ('Cat' to 'IEF'); MSP-parameters and results ('Type' to 'Change'); and the ratio of the Thellier- and the MSP results expressed as a percentage (e.g. a ratio of +10 per cent implies that the results of the Thellier palaeointensity experiment is 10 per cent higher than the results of the MSP experiment on the same site). The Thellier parameters include (from left to right): category indicator (Cat; see main text), the temperature range used (ΔT), the number of samples (N), the angle between the origin-anchored and floating line fits in the Zijderveld plot (α); the fraction (f), gap (g) and quality (q) factors (Coe 1978); the fraction of the standard error of the slope of the line fit and the slope (β); the difference ratio DRAT (Selkin & Tauxe 2000); the obtained palaeointensity (PI); the one-standard-deviation error and the Intensity Error Fraction (IEF). The MSP-parameters include (from left to right): the type of the experiment (DB or DSC; in air or in argon; fast or slow cooling rate; or the steps for the viscosity experiments with indication whether the strict (s) or random (r) time regime was used (see main text)); the number of samples used (number of samples rejected between brackets); the slope (a), *y*-axis intercept (b) and the coefficient of determination (r^2) of the linear fit; the obtained palaeointensity (PI), the one-standard-deviation confidence interval of the line fit (error); the IEF; and the percentage change in obtained palaeointensity with respect to the MSP-DB results for repeated MSP-style experiments with changed boundary conditions (e.g. experiments in argon, with a different cooling rate, or repeated experiments to test for viscosity) for the same site.

			Thellier											MSP									
Site	G	Cat	ΔT (°C)	N	α	f	g	q	β	DRAT	PI (μT)	Error	IEF	Type	n	a	b	r^2	PI (μT)	Error	IEF	Change (per cent)	Ratio (per cent)
23-1A	–	A	20–280	7	0.7	0.65	0.75	5.8	0.08	13.3	28.3	2.4	−32.9										
23-1B	L	F												DB	15	0.0175	0.5301	0.947	30.3	[26.3–33.7]	−28.2		
														DSC	5	0.0506	1.3150	0.992	26.0	[20.6–30.3]	−38.4	−4.2	
23-1C	L	B	100–280	6	9.0	0.57	0.63	3.3	0.11	14.7	27.2	3.0	−35.7	in air	11 (1)	0.0126	0.4216	0.856	33.4	[24.8–41.0]	−20.9		−18.7
														in argon	11	0.0134	0.4926	0.868	36.9	[29.7–44.6]	−12.6	10.5	−26.4
23-2	C	B	20–280	8	9.5	0.42	0.81	2.3	0.15	14.7	45.9	6.9	8.7										
71-1	L	B	20–280	8	11.6	0.59	0.75	3.3	0.13	19.1	32.3	4.3	−26.4	DB	23 (1)	0.0150	0.4894	0.941	32.7	[30.0–35.1]	−25.5		−0.9
														DB @160°C	18	0.0104	0.2945	0.918	28.3	[23.9–31.9]	−35.5	−13.2	14.1
														DSC	5 (1)	0.0255	0.7354	0.951	28.8	[1.5–40.5]	−34.4	−11.7	12.2
71-2A	C	B	20–280	8	12.0	0.56	0.76	3.2	0.13	18.2	38.8	5.2	−11.6	DB	18	0.0125	0.3731	0.959	29.8	[26.7–32.6]	−32.1		30.3
														DSC	5 (1)	0.0372	0.9244	0.995	24.9	[19.6–28.9]	−43.3	−16.4	55.9
71-2B	L	A	20–280	8	8.8	0.43	0.80	3.4	0.10	13.8	37.7	3.9	−14.1	DB	10	0.0144	0.5082	0.938	35.3	[30.8–40.2]	−19.6		6.9
														in argon	12	0.0122	0.4631	0.880	38.0	[31.2–45.0]	−13.4	7.6	−0.7
														II (r)	10 (1)	0.0137	0.5606	0.968	41.0	[37.8–44.3]	−6.6	16.1	
														III (r)	8	0.0136	0.5102	0.935	37.5	[32.4–44.8]	−14.6	6.2	
														IV (r)	8	0.0121	0.5061	0.912	41.7	[35.2–52.3]	−5.0	18.1	
71-2C	-	H	20–340	9	3.9	0.19	0.75	1.7	0.08	20.3	35.4	3.0	−19.3										
71-3A	-	A	20–340	9	6.1	0.79	0.85	6.6	0.10	11.9	29.2	3.0	−33.6										
71-3B	-	A	20–280	8	7.4	0.68	0.81	5.5	0.10	11.2	34.0	3.5	−22.5										
71-3C	L	A	20–340	9	11.4	0.68	0.85	6.7	0.09	7.0	24.1	2.1	−45.1	DB	20	0.0152	0.4429	0.974	29.2	[27.2–31.2]	−33.5		−17.5
														II (s)	20	0.0156	0.4568	0.976	29.3	[27.3–31.1]	−33.3	0.3	
														III (s)	20	0.0157	0.4558	0.978	29.0	[27.2–30.8]	−33.9	−0.7	
														IV (s)	20	0.0156	0.4596	0.978	29.4	[27.6–31.1]	−33.0	0.7	
79-1A	C	2sl	150–340	6	10.9	0.51	0.77	4.2	0.09	17.3	17.5	1.7	−60.3										
79-1B	L	B	20–280	8	4.1	0.61	0.76	5.8	0.08	18.3	30.0	2.4	−32.0										
79-1C	-	H	20–340	9	6.3	0.22	0.74	2.0	0.08	8.9	33.2	2.8	−24.8										
83-1A	H	F																					
83-1B	H	F												fast	15 (2)	0.0046	0.1231	0.938	27.0	[24.2–30.2]	−38.9		
														slow	7	0.0039	0.0958	0.910	24.3	[12.2–31.6]	−45.0	−10.0	

Table 2. (*Continued.*)

Site	G	Cat	ΔT (°C)	N	Thellier α	f	g	q	β	DRAT	PI (μT)	Error	IEF	Type	MSP n	a	b	r^2	PI (μT)	Error	IEF	Change (per cent)	Ratio (per cent)
83-1C	H	F												fast	9	0.0059	0.1717	0.954	29.1	[27.1–31.5]	−34.2		
														slow	7	0.0043	0.1089	0.931	25.4	[15.9–31.8]	−42.5	−12.7	
83-1D	H	F												fast	15 (1)	0.0061	0.1763	0.934	29.1	[26.4–32.0]	−34.2		
														slow	9	0.0072	0.1845	0.840	25.6	[13.5–32.6]	−42.1	−12.0	
83-1E	H	F												fast	15 (1)	0.0065	0.1580	0.953	24.4	[22.0–26.8]	−44.8		
														slow	7	0.0082	0.1526	0.855	18.5	[0.9–27.4]	−58.1	−24.2	
83-2	H	C	20–340	9	11.2	0.38	0.76	1.7	0.17	16.3	28.3	4.7	−36.0										
83-3	H	C	100–280	7	6.1	0.24	0.64	0.7	0.24	46.1	35.3	8.3	−20.1	DB	23 (1)	0.0093	0.3190	0.904	35.0	[30.6–37.4]	−20.8		3.2
														DB @ 160°C	18	0.0066	0.1855	0.942	27.9	[24.4–31.0]	−36.9	−18.4	26.6
														DSC	5 (1)	0.0911	2.2973	0.948	25.2	[0–42.2]	−43.0	−26.3	40.1
83-4A	C	C	100–280	7	9.8	0.49	0.83	1.9	0.21	25.4	25.6	5.3	−42.0	DB	20 (2)	0.0082	0.2105	0.766	25.7	[18.4–32.5]	−41.9		−0.2
														II (s)	20 (2)	0.0089	0.2370	0.765	26.7	[19.4–33.5]	−39.6	3.9	
														III (s)	20 (2)	0.0088	0.2299	0.751	26.1	[18.5–33.2]	−41.0	1.6	
														IV (s)	20 (2)	0.0091	0.2434	0.784	26.7	[19.9–33.1]	−39.6	3.9	
83-4B	L	C	100–280	7	9.5	0.48	0.80	1.3	0.29	25.9	27.0	7.7	−39.0	DB	12	0.0161	0.4956	0.950	30.8	[26.3–35.0]	−30.3		−12.4
														in argon	12	0.0145	0.4123	0.964	28.4	[24.5–32.0]	−35.7	−7.8	−5.0
														II (r)	10	0.0146	0.4618	0.951	31.6	[26.4–35.8]	−28.5	2.6	
														III (r)	8	0.0220	0.6013	0.956	27.4	[23.8–31.5]	−38.0	−11.0	
														IV (r)	8	0.0196	0.6081	0.975	31.1	[28.3–34.4]	−29.6	1.0	
83-4C	C	2sl	150–340	6	13.5	0.41	0.70	2.5	0.12	33.4	15.3	1.8	−65.4										
83-5	L	2sl	130–280	6	8.8	0.30	0.80	1.5	0.16	32.9	15.5	2.4	−64.9										
83-6	C	C	130–280	6	8.8	0.30	0.80	1.5	0.16	32.9	15.5	2.4	−64.9	DB	15 (1)	0.0156	0.4784	0.943	30.6	[26.3–34.3]	−30.8		−49.3
														DSC	5	0.0614	1.2386	0.877	20.2	[0–36.0]	−54.3	−34.0	−23.2
02-1A	C	F																					
02-1B	H	F																					
02-1C	H	B	100–280	7	8.1	0.44	0.72	2.5	0.12	18.7	42.8	5.3	−4.2	DB	5 (1)	0.0083	0.2249	0.914	27.2	[0–43.9]	−39.1		57.4
														DSC	5 (1)	0.0286	0.7009	0.936	24.5	[0–37.9]	−45.2	−9.9	74.8
02-2	H	B	20–280	8	12.9	0.48	0.75	3.1	0.12	15.9	31.0	3.7	−30.6	DB	10 (2)	0.0163	0.4868	0.945	29.8	[23.8–34.7]	−33.3		4.1
														DSC	5	0.0672	1.8039	0.983	26.8	[18.7–32.7]	−40.0	−10.1	15.8
02-3	H	F																					
23-1A TRM														in air	9	0.0112	0.3967	0.974	35.4	[31.6–39.1]	−11.5		
														in argon	9 (1)	0.0121	0.4522	0.995	37.3	[35.7–39.0]	−6.8	4.8	
79-1A TRM														in air	12	0.0062	0.2021	0.950	32.4	[28.0–36.6]	−19.0		
														in argon	12 (4)	0.0072	0.2543	0.979	35.1	[32.5–38.0]	−12.3	8.3	
83-4C TRM														in air	11 (1)	0.0090	0.3040	0.964	33.9	[29.8–37.8]	−15.3		
														in argon	11 (5)	0.0880	0.3088	0.978	35.1	[30.6–39.4]	−12.3	3.5	

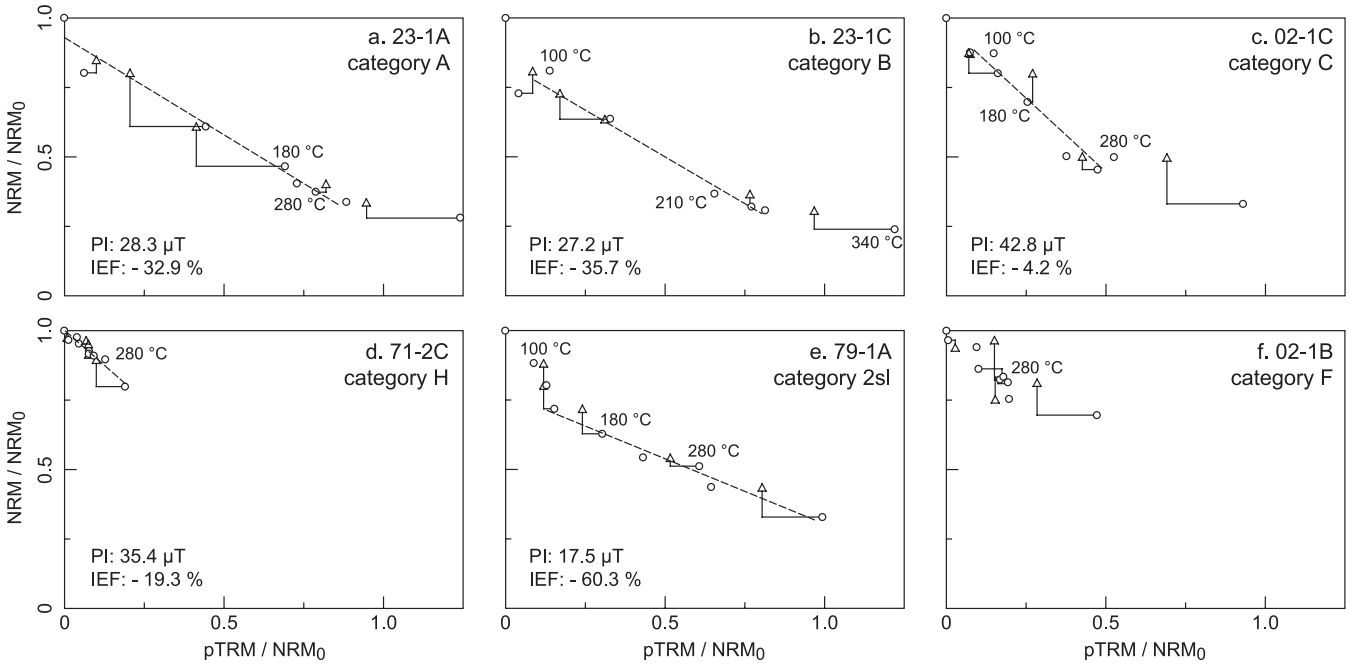

Figure 3. Typical Thellier results. An example of each category of the Thellier results distinguished (see main text) is given. Open circles indicate the Thellier experiment data; open triangles the pTRM checks. A dashed line indicates the linear fit. The obtained palaeointensity and the IEF are given in the lower left corner.

of samples used in the experiment and the variation among samples; the confidence interval in absolute terms is generally less than $\pm 5\mu$T. For sites 71-1 and 83-3 the MSP-DB experiment was done at two set temperatures: 160°C and 250°C. For both sites this results in notably different results, with the lowest temperature yielding lowest palaeointensities: 28.3 versus 32.7 μT for site 71-1 and 27.9 versus 35.0 μT for site 83-3. Apparently the set temperature used in the MSP-DB experiments influences the outcome for these flows. The average IEF of the MSP-DB experiments differs significantly among the rock-magnetic groups. Rock-magnetic group L has an average IEF of -26.4 ± 5.4 per cent (six sites), group H an average IEF of -35.5 ± 6.9 per cent (six sites) and group C yields -34.9 ± 6.0 per cent (six sites). Groups H and C are indistinguishable, but underestimate the palaeofield significantly more than sites from rock-magnetic group L.

4.3.2 Tail corrected MSP experiment

The MSP-DSC protocol (Fabian & Leonhardt 2010) was applied to seven sites in this study (Fig. 4). As expected from the phenomenological theory (Fabian & Leonhardt 2010) all MSP-DB results are lowered even further, yielding palaeointensities that are between 9.9 and 34.0 per cent lower than the MSP-DB results. The MSP-DSC protocol should reduce the scatter for an equal number of specimens because subtle differences in domain state are corrected for (Fabian & Leonhardt 2010). Therefore, a tighter one-standard-deviation error envelope is to be expected. However, the experiments following the MSP-DSC protocol in this study were done with fewer samples than the MSP-DB protocol experiments. Hence, the error envelope around the fit is usually broader for these results compared to the MSP-DB results.

4.3.3 Testing for subtle chemical alteration

Samples from sites 23-1C, 71-2B and 83-4B were subjected to the MSP-DB in argon experiment. The obtained palaeointensities from the experiments in argon are all within the one-standard-deviation error envelopes of the results of the experiments in air and vice versa (Figs 5a–c, Table 2). The full laboratory TRM MSP-DB experiments in air with samples from sites 23-1C, 79-1A and 83-4C yield underestimates of the field used: 35.4 μT (23-1C), 32.4 μT (79-1A) and 33.9 μT (83-4C) where 40 μT is expected (Figs 5d–f). The sister specimens subjected to the full laboratory TRM MSP-DB experiment in argon yield estimates that are closer to the imparting field. However, they are still underestimates: 37.3 μT for site 23-1C and 35.1 μT for sites 79-1A and 83-4C.

4.3.4 Testing for viscous behaviour

For sites 71-2B and 83-4B, the MSP-DB experiments were repeated using the 'random time' regime; samples from sites 71-3C and 83-4A were subjected to repeated MSP-DB experiments in the 'strict time' regime (both with the NRM as starting TRM). Both time regimes yield different results in terms of scatter and reproducibility (Fig. 6). Measuring the samples again after storing them randomly in the Earth's magnetic field for two weeks, yields a significant increase of the palaeointensity for site 71-2B, its palaeointensity increases from 35.3 (step I) to 41.0 μT (step II), an increase of 16 per cent. Repeating the MSP-DB experiment (step III) decreases the palaeointensity estimate to 37.5 μT, well within the error envelope of step I measurements. In the final step, step IV, the error envelope of the fit increases, due to unexplained spreading in the data points. For the other site, 83-4B, the obtained palaeointensity after two weeks (31.6 μT, step II) and after repeating the experiment twice [27.4 (step III) and 31.1 μT (step IV)] does not differ significantly from the palaeointensity measured directly after the first heating of the samples [30.8 μT (step I)].

The strict time regime experiments show remarkably small changes in results for each step. For site 71-3C the changes in obtained palaeointensity are within 1 per cent compared to the first experiment (29.2 μT). For site 83-4A the changes are slightly larger

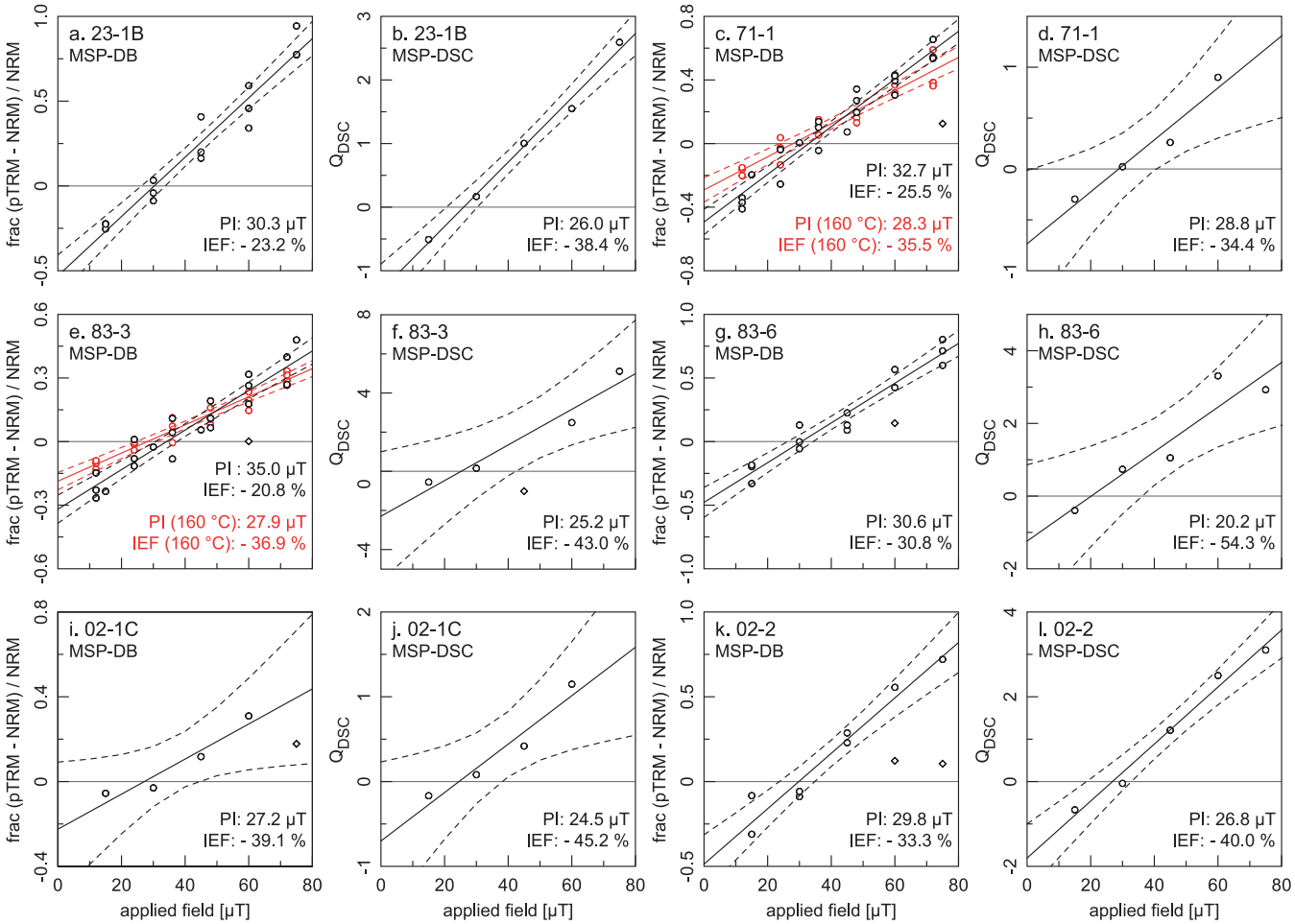

Figure 4. MSP-DB and MSP-DSC results. The MSP-DB (left-hand side) and the MSP-DSC results (right-hand side) for the same sites are given. The data points (open circles), linear fit (solid line) and the one-standard-deviation error envelope (dashed lines) are indicated. Omitted data points are depicted as open diamonds. The obtained palaeointensity and the IEF are given in the lower right-hand corner of each panel. For sites 71-1 and 83-3 the MSP-DB experiment was done at two temperatures: 160 and 250°C, the experiment at 160°C is indicated in red, the experiment at 250°C in black.

but still within 4 per cent compared to the first experiment that yields 25.7 µT. For both sites, the measured remanence for individual samples does not vary more than 5 per cent between all steps.

4.3.5 Cooling rate effects

Cooling rate experiments were carried out with samples from site 83-1. The MSP-DB protocol for sites 83-1B to 83-1E with a fast (laboratory) cooling rate again appear to deliver underestimates of the palaeofield: with increasing depth 27.0, 29.1, 29.1 and 24.4 µT are obtained (Figs 7 and 8). These differences, however, are small. It is noteworthy that the parts of the block with a slower natural cooling rate yield higher palaeointensities than the parts of the block that experienced a faster natural cooling rate. It is also noteworthy that the MSP-DB experiment with a slow laboratory cooling rate of 10.8 K/day yields lower palaeointensity results than the experiments with a fast laboratory cooling rate. Samples taken 45, 90 and 133 cm below the top of the flow, lines 83-1B, -1C and -1D, respectively, yield palaeointensities that are 10.0–12.7 per cent lower than those obtained from samples that are cooled quickly (24.3 versus 27.0 µT for the line 45 cm below the top; 25.4 versus 29.1 µT for the line at 90 cm; and 25.6 versus 29.1 µT for the line at 133 cm). The lowermost samples (taken 168 cm below the top) yield a palaeointensity that is 24.2 per cent lower when cooled slowly: 18.5 versus 24.4 µT (Fig. 8). Due to the lower number of samples used in the slow cooling-rate experiments, the one-standard-deviation error envelope of these fits is wider than the one-standard-deviation error envelope of the fast-cooled samples. Therefore, the results of the slow-cooled samples are outside the error envelope of the fast cooled samples, and thus significantly different; but the result of the fast-cooling rate experiments are within the error envelope of the slow-cooled samples.

5 DISCUSSION

All MSP-style experiments and all but one Thellier-style experiments yield underestimates of the palaeofield. This concurs with earlier observations by Hill & Shaw (1999), Calvo *et al.* (2002) and Biggin *et al.* (2007a). In this study we changed the experimental conditions of the MSP-style experiments in an attempt to uncover a reason for the underestimates. We now assess the influence of several parameters on the obtained palaeointensity values: after a brief recapitulation of the Thellier-style and MSP-style results, the influence of subtle chemical alteration, viscosity and changing the laboratory cooling rate are reviewed.

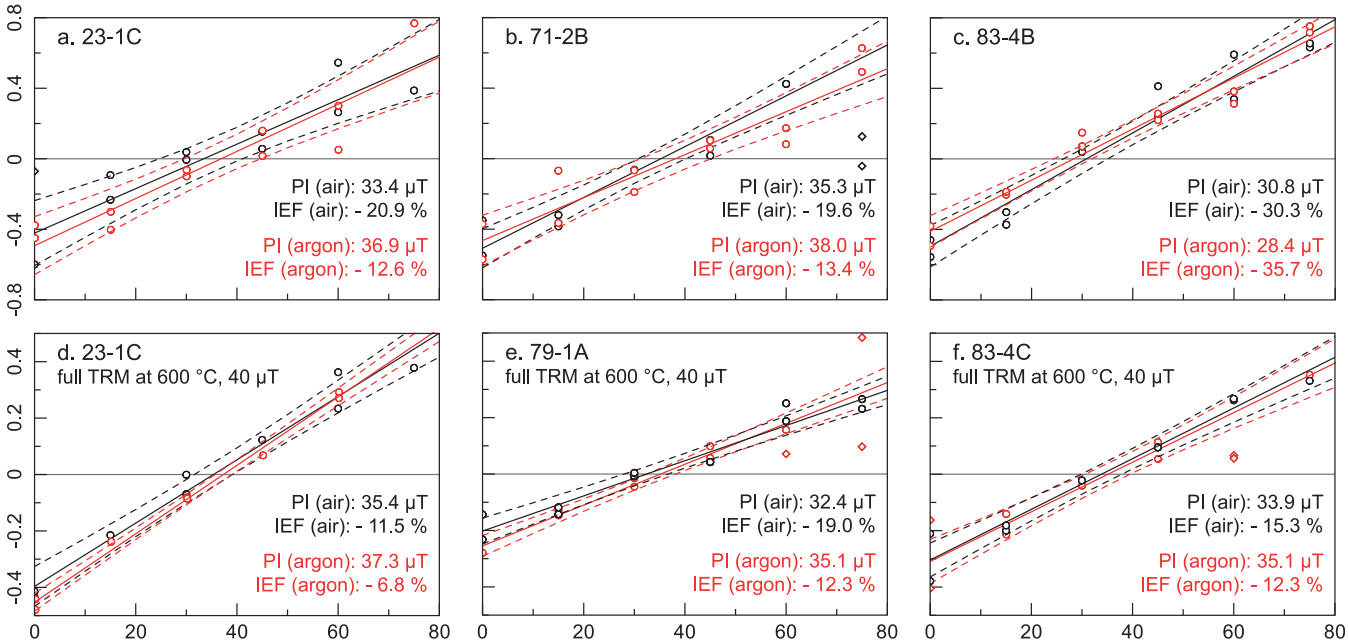

Figure 5. MSP-DB results in air and in argon. The top row of panels gives the results of experiments in air (black) and in argon (red) on pristine samples containing the natural NRM as TRM. The bottom row gives the results of the MSP-DB experiments in air (black) and in argon (red) on samples that were first given a full TRM at 600°C in a field of 40 μT. The data points (open circles), the linear fit (solid line), the one-standard-deviation error envelope (dashed lines) are indicated. Omitted data points are depicted as open diamonds. The obtained palaeointensities and IEFs are indicated in the lower right-hand corner of each panel.

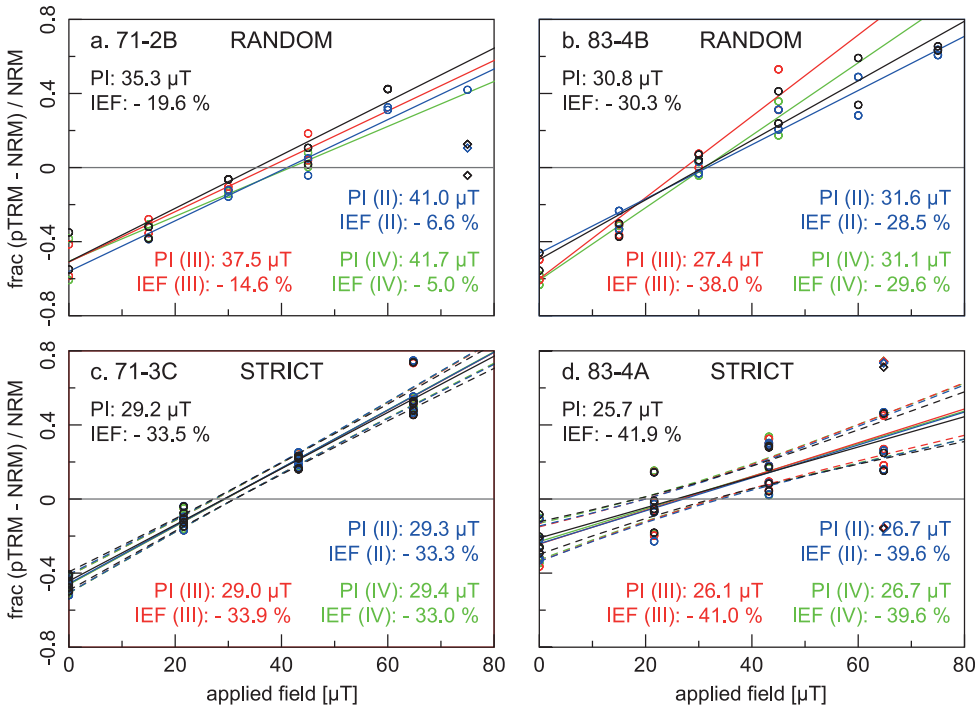

Figure 6. Viscosity tests for the MSP-DB results. Sites 71-2B and 83-4B were subjected to the random time regime (see main text), sites 71-3C and 83-4A were subjected to the strict time regime. Data points are depicted as open symbols, linear fits as solid lines, one-standard-deviation error envelopes (for the samples in the strict time regime) as dashed lines. Omitted data points are depicted as open diamonds. The results of the first MSP-DB experiment are in black, the second step (step II) in blue, the third step (step III) in red and the fourth step (step IV) in green. Obtained palaeointensities and IEFs for all experiments are also indicated. Note the differences in spreading between the random and strict time regimes.

5.1 Thellier results

For comparison with MSP-style outcomes and the IGRF we interpreted Thellier results that would normally not be considered by an interpreter (category B and certainly categories C, H and 2sl). In rock-magnetic group H only a small portion of the NRM is unblocked. As this portion is 200–300°C lower than the dominant Curie temperature, this results in a low f-factor. This may

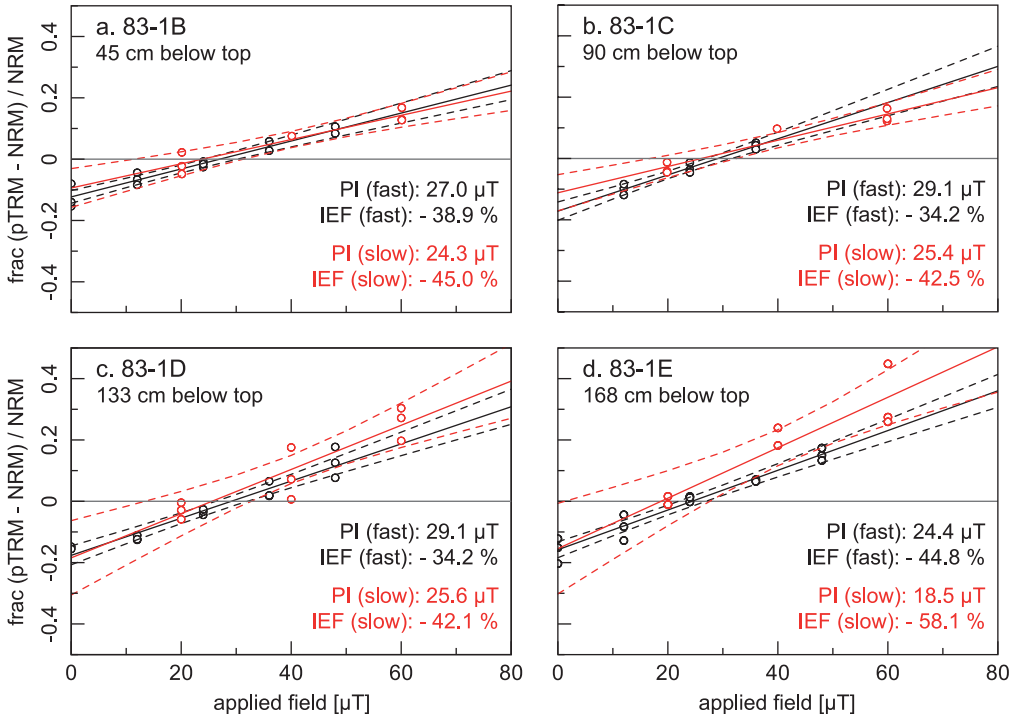

Figure 7. Cooling rate experiments. The results of experiments using a slow cooling rate of 10.8 K/day are indicated in red, the results of the experiments using the fastest possible laboratory cooling rate (15–20 K/min) are indicated in black. Open circles indicate the data points, the solid lines the linear fits and the dashed lines the one-standard-deviation error envelopes. The sample 'line' and the distance to the top of the flow are in the top left-hand corner of each panel; the obtained palaeointensity and IEFs for both experiments are in the respective lower right-hand corners.

explain the failure to reconstruct the IGRF field accurately, although Herrero-Bervera & Valet (2009) reported lavas being characterized by a single high Curie temperature to produce the best results. Two-slope behaviour is not straightforwardly explained in these samples: a large viscous remanent magnetization (VRM) is unlikely to be present (historic lavas). The two-slope behaviour might arise from differences in the composition of the magnetic mineralogy or be a consequence of magnetic domain-state effects in PSD and MD particles.

5.2 Thellier versus MSP results—some considerations

It is remarkable that essentially all samples yield underestimates of the palaeofield in Thellier-style experiments. Such samples acquire 'too much' pTRM for a given temperature range (the range with which the line fit in the Arai plot is calculated). This decreases the slope of the fit in the Arai plot, and thus lower the palaeointensity estimate. In MSP-style experiments, samples that acquire too much pTRM steepen the slope of the line fit in the scaled pTRM fraction versus field intensity plot. However, the *y*-axis intercept in that plot—*de facto* determined by a demagnetization step of the NRM at the set temperature (pTRM acquisition field is 0 μT)—is not changed. Therefore samples that acquire too much pTRM produce underestimates of the palaeofield in MSP-style experiments as well as in Thellier-style experiments. This is fully corroborated by our results. Therefore, observed trends in IEF changes and changed boundary conditions in the MSP-style experiments are expected to be similar for Thellier experiments that would have been subjected to the same boundary conditions. In other words we may extrapolate the MSP results to Thellier-style experiments. Some caution, however, is required since the MSP-style experiments rely on one single temperature during the experiment. It is conceivable that the effects of changing experimental boundary conditions are temperature-dependent. In those cases the results of Thellier-style experiments might be affected differently.

5.3 Testing for subtle chemical alteration

Pristine samples (with the NRM as full TRM) yield the same palaeointensity results independent of heating atmosphere: MSP-DB in argon is equivalent to MSP-DB in air. So, the observed palaeointensity underestimates cannot be explained by variations in the oxygen fugacity of the heating atmosphere in the furnace. However, the oxygen fugacity within the samples, in the direct vicinity of the Fe-Ti-oxides, need not be the same as that of the furnace atmosphere outside the samples. Also thermally driven unmixing of titanomagnetite into a magnetite-rich and ilmenite-rich end-member could still be invoked as possible causes of the observed underestimates.

The MSP-DB experiments on samples with a full laboratory TRM (acquired in an argon atmosphere) should be insightful pertaining to clarifying the aforementioned processes. Because the full TRM in the samples is imparted at 600°C, thermochemical processes like oxy-exsolution or unmixing will occur during TRM acquisition if the samples are prone to these processes. Because thermochemical alteration processes are ∼10 orders of magnitude slower at 250° than at 600°C—if they occur at all at that temperature after samples having been heated to 600°C—reheating the samples to 250°C in a (MSP) palaeointensity experiment should approximately reconstruct the laboratory full TRM acquisition field. The MSP-DB experiments on these samples, however, also yield underestimates of the palaeofield, albeit with smaller IEFs than in the experiments on samples with their NRM. For the experiments done in air, the TRM acquisition field is underestimated by between 11.5

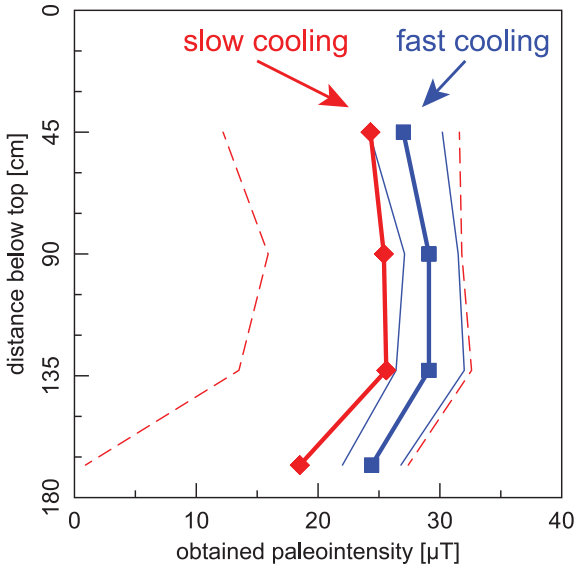

Figure 8. Cooling rate profile of site 83-1. The distance from the top of the block is plotted on the vertical axis, the obtained palaeointensity on the horizontal axis. The results obtained from the experiments using the fast laboratory cooling rate are indicated in blue: the palaeointensities are the squares connected by the thick line, the one-standard-deviation error envelope is indicated by the thin lines. The results obtained using the slow cooling rate are in red: the diamonds are the obtained palaeointensities and are connected by the thick line, the one-standard-deviation error envelope is indicated by the thin dashed lines.

and 19.0 per cent. The results of the MSP-DB experiments in argon are closer to the TRM acquisition field: IEFs range between −6.8 and −12.3 per cent. The samples appear to be sensitive to the furnace atmosphere at 250°C after having been heated to 600°C for the TRM acquisition. The Fe-Ti oxides are subject to thermochemical alteration at high temperature and are envisaged to be partially quenched during cooling from 600°C. This process makes the samples apparently sensitive to the ambient atmosphere in the furnace during the MSP-DB experiments. The experiments in air seem to be slightly more prone to oxy-exsolution that leads to a higher pTRM capacity, indicating more fine-grained titanium-poor magnetite. This results in a larger underestimate. Because this process is only observed to some extent in the samples that are given a full laboratory TRM, it is not a likely cause for the observed underestimates in the palaeointensity experiments with pristine sample material.

5.4 Testing for viscous behaviour

The experiments in which the MSP experiments are repeated reveal that viscous behaviour on laboratory timescales can be an issue in some of the samples as reported earlier by Biggin *et al.* (2007a), but the effect of the viscous behaviour is less than 10 per cent—insufficient to explain the observed underestimates. Furthermore, the viscous behaviour effects can be avoided by enforcing a strict time regime while carrying out the experiments.

5.5 Cooling rate effects

As suggested by Hill & Shaw (1999) and Biggin *et al.* (2007a), differences between the natural and laboratory cooling rates may be a plausible cause of the observed deviations of the obtained palaeointensities from the expected IGRF values. Temperature-time profiles have been measured in cooling lavas and can be incorporated in heat-flow models. The first large data sets on temperature profiles in cooling lava were presented by Wright & Okamura (1977) and Peck (1978) who studied two tholeiitic Hawaiian lava lakes. The observed cooling rates were modelled by Peck *et al.* (1977) and Shaw *et al.* (1977). Hon *et al.* (1994) extended the temperature profile database for lavas; they report a quadratic relation between the crustal thickness of the flow and the time needed to cool to solidification temperature (that is well above the range of temperatures at which the NRM is blocked). The elaborate 'FLOWGO' model (Harris & Rowland 2001) for the (thermal) behaviour of a lava flow considers more than 40 parameters. The model is applied to three case studies including the 1998-flow of Mt Etna; a typical cooling rate of 5.0×10^{-2} to 1.0×10^{-3} K min^{-1} (8.3×10^{-4} to 1.7×10^{-5} K s^{-1}) is reported for these flows. The cooling rate in our experiments was set at 1.25×10^{-4} K s^{-1}, well within this natural cooling-rate range. The differences of the cooling rate within a flow are described by Kattenhorn & Schaefer (2008). A flow cools most efficiently from the top, but also looses some of its heat to the underlying strata. The slowest cooling parts are reported at approximately two-thirds of the thickness of the flow, measured from the top. For site 83-1 this corresponds to a depth of approximately 120 cm from the top. It would imply that lines 83-1C and 83-1D (at 90 and 133 cm from the top) cooled the slowest and with approximately the same rate. Lines 83-1B and 83-1E (45 and 168 cm from the top) cooled slightly faster.

In the cooling rate profile (Fig. 8) the lines with the highest natural cooling rate (lines 83-1B and 83-1E) underestimate the palaeofield more than the samples with a lower natural cooling rate (lines 83-1C and 83-1D). If the difference in cooling rate would be the major cause of the observed underestimates, the results of the slow cooling rate experiments are anticipated to provide a better estimate of the expected IGRF value than the experiments using a fast laboratory cooling rate. However, the opposite is observed: the results with a slow laboratory cooling rate yield even lower palaeointensities (i.e. larger underestimates) than the experiments with a fast laboratory cooling rate. Furthermore, the smallest palaeointensity underestimates are obtained from samples that experienced a fast laboratory cooling rate but that had the slowest natural cooling rate: samples from the central part of the lava flow. Although the cooling rate used in the MSP-DB experiment influences its outcome, the measured underestimates are not caused by cooling rate differences as sole factor.

For SD grains, theory and observations predict overestimates of the palaeofield in Thellier-style experiments (and therefore in MSP-style experiments as well as argued before; Dodson & McClelland-Brown 1980; Halgedahl *et al.* 1980; Walton & Williams 1988). The intensities of (p)TRMs that are imparted using a faster cooling rate than the cooling rate in which the NRM was acquired, are lower for SD grains. If the results of palaeointensity experiments are not corrected for this effect, both Thellier and MSP experiments, therefore, overestimate the palaeofield. Thus by theory, SD samples that are cooled slower while imparting the pTRMs yield better estimates of the palaeofield (a smaller overestimate) than the faster cooled samples. The imparted pTRM is higher for a slower (laboratory) cooling rate and therefore more similar to the unblocked portion of the NRM, if the laboratory field is equal to the NRM imparting field. The cooling rate effect in true MD particles is occasionally reported to be the opposite of the effect observed in SD grains: MD grains yield lower TRMs for slower cooling rates (McClelland-Brown 1984; Perrin 1998) and would therefore lead to underestimates in both

Thellier- and MSP experiments. The theory for these grain sizes, however, is poorly understood. For PSD grains, Yu (2011) experimentally showed that the influence of the cooling rate on acquired pTRMs is insignificant. His two cooling rates compare to the fast cooling rate used in this study. If Yu's (2011) results can be extrapolated to distinctly lower cooling rates it would imply that the outcome of the palaeointensity experiment is only marginally influenced by the cooling rate for the PSD portion of the particle suite.

Rock-magnetic group H—to which all samples used in the cooling rate experiments belong—shows a broad range of titanomagnetite compositions. The dominant grain size indicated by preliminary rock-magnetic experiments is PSD so a mere extrapolation of either SD or MD inferences is not warranted. Although (slightly) lower palaeointensities are observed for the slower cooled samples—in line with SD theory—SD theory predicts overestimates, which are not found. Furthermore, the samples that cooled with a similar rate in the laboratory as in nature should yield approximately the correct palaeointensity. This is not observed: slow cooling yields larger underestimates. Therefore, the contribution of SD particles to the NRM cannot be large: substantial underestimates are observed which are even enlarged in the slow cooling rate experiments. MD theory predicts underestimates of the palaeofield—in line with the results presented here—but this MD cooling rate effect cannot explain the observed underestimates. True MD grains contribute less to the bulk (p)TRM intensity of the samples than PSD and SD grains, but their presence would be revealed by high-field rock-magnetic experiments (e.g. a Day plot)—which prominently indicate the presence of PSD grains. MD cooling rate effects are therefore deemed insignificant for these samples. The effect of the experimental cooling rate on PSD grains is not very well understood. If Yu's (2011) results may be extrapolated to the cooling rates we have used in our experiments, large changes in the palaeointensity results are not expected. However, the results of the slow-cooled samples are on average ∼10 per cent lower than those of the fast-cooled samples. This effect is therefore deemed secondary since the palaeofield is underestimated by ∼30–45 per cent using these samples. The observed underestimates of the palaeofield can thus not be straightforwardly explained by differences in cooling rate in nature and during the palaeointensity experiment.

5.6 Magnetic domain-state changes

Each of the boundary conditions tested in this study cannot be put forward as the prime reason for the anomalously low palaeointensities obtained from recent Mt Etna flows. Although both viscous magnetic behaviour and differences in cooling rate do influence the outcome of the palaeointensity experiments, the trend in and the magnitude of the effects do not yield satisfactory explanations. Four subsites included in this study (23-2, 71-3C, 79-1 and 83-4A) were previously subject of a study by de Groot *et al.* (2012). In that study the acquired anhysteretic remanent magnetization (ARM) is isolated from the demagnetizing NRM. This is done for two groups of sister specimens: (1) pristine samples in their NRM magnetic state and (2) samples that were heated in zero field to the temperature used in the MSP-DB experiment. The purpose of this protocol is to be able to evaluate the effects of subtle changes in magnetic state. ARM acquisition curves are capable of reflecting such changes. All samples from Mt Etna appear to acquire more ARM after heating the samples to the MSP set temperature. This is perfectly in line with the observed underestimates, since samples that yield an underestimate acquire 'too much' pTRM after the heating step. After the experiment outlined above (de Groot *et al.* 2012) both groups (the group that was heated and the group that was not) were given a full 3-axes AF demagnetization at 300 mT after which the ARM acquisition curve was measured again. After this full AF demagnetization step the observed changes in the behaviour of the ARM acquisition are removed for sites 71-3C, 79-1 and 83-4A: the ARM acquisition curves for the non-annealed and annealed groups are now the same. For site 23-2 the differences in the ARM acquisition curves appeared to be even more pronounced which was tentatively attributed to very incipient thermochemical alteration. All in all, this implies that for the first three sites the effect that probably causes the palaeointensity underestimates can be fully undone with AF demagnetization. Therefore, it must have a magnetic origin (it cannot be thermochemically since AF demagnetization removes the effect). Further it is very subtle in character. Transdomain transitions from one local energy minimum state to another would be a plausible option.

6 CONCLUSIONS

Technically acceptable palaeointensity data obtained from samples of Mt Etna presented here generally yield underestimates of the palaeofield; that is, the samples acquire more magnetization while imparting a pTRM in the laboratory than during the recording of the NRM in the same external magnetic field. This is in agreement with previous findings by Hill & Shaw (1999), Calvo *et al.* (2002) and Biggin *et al.* (2007a). Based on the rock-magnetic analyses and palaeointensity experiments in argon and the experiments on the samples that were subjected to a laboratory-imparted full TRM, subtle chemical alteration can be ruled out as a cause. Although the samples do show signs of moderate viscous behaviour after heating, both the magnitude and the expected influence of viscosity on the outcome of palaeointensity experiments make viscosity not a prime culprit to explain the observed underestimates. Differences between the natural and laboratory cooling rate do have an effect on the results of the palaeointensity experiments, but—counter-intuitively—the obtained palaeointensities using a cooling rate in the laboratory that is in the order of the natural cooling rate underestimates the palaeofield even further. Transdomain transitions are suggested to be an explanation for these large underestimates of up to 30–40 per cent, stronger than the effects calculated for local magnetic field anomalies due to uneven lava surfaces.

ACKNOWLEDGEMENTS

We thank Andy Biggin for his help in the field and for his helpful comments and discussions. Stefano Branca is gratefully acknowledged for providing the DEM map of the Etna region (Fig. 1). Yongjae Yu and two anonymous reviewers are acknowledged for their thorough and constructive reviews, which greatly helped to improve this manuscript. *In memoriam* Tom Mullender—His encouragements, support and passion for innovative solutions are deeply missed.

FUNDING

This research was funded by a grant from the Earth and Life Science Division (ALW) of the Netherlands Organization for Scientific Research (NWO). The robotized 2G SQUID magnetometer was developed with support of the instrument fund of NWO.

REFERENCES

Aitken, M., Allsop, A., Bussell, G. & Winter, M., 1988. Determination of the intensity of the Earth's magnetic field during archaeological times: reliability of the Thellier technique, *Rev. Geophys.,* **26,** 3–12.

Baag, C., Helsley, C.E., Xu, S. & Lienert, B.R., 1995. Deflection of paleomagnetic directions due to magnetization of the underlying terrain, *J. geophys. Res.,* **100,** 10 013–10 027.

Biggin, A. & Böhnel, H., 2003. A method to reduce the curvature of Arai plots produced during Thellier palaeointensity experiments performed on multidomain grains, *Geophys. J. Int.,* **155,** F13–F19.

Biggin, A.J., Perrin, M. & Dekkers, M.J., 2007a. A reliable absolute palaeointensity determination obtained from a non-ideal recorder, *Earth planet. Sci. Lett.,* **257,** 545–563.

Biggin, A.J., Perrin, M. & Shaw, J., 2007b. A comparison of a quasi-perpendicular method of absolute palaeointensity determination with other thermal and microwave techniques, *Earth planet. Sci. Lett.,* **257,** 564–581.

Bowles, J., 2005. Cooling rate effects on paleointensity estimates in submarine basaltic glass and implications for dating young flows, *Geochem. Geophys. Geosyst.,* **6,** doi:10.1029/2004GC000900.

Calvo, M., Prévot, M., Perrin, M. & Riisager, J., 2002. Investigating the reasons for the failure of palaeointensity experiments: a study on historical lava flows from Mt. Etna (Italy), *Geophys. J. Int.,* **149,** 44–63.

Coe, R.S., 1967. Paleo-intensities of the Earth's magnetic field determined from Tertiary and Quaternary rocks, *J. geophys. Res.,* **72,** 3247–3262.

Coe, R.S., 1978. Geomagnetic paleointensities from radiocarbon-dated lava flows on Hawaii and the question of the Pacific nondipole low, *J. geophys. Res.,* **83,** 1740–1756.

Cottrell, R.D. & Tarduno, J.A., 1999. Geomagnetic paleointensity derived from single plagioclase crystals, *Earth planet. Sci. Lett.,* **169,** 1–5.

Day, R., Fuller, M. & Schmidt, V., 1977. Hysteresis properties of titanomagnetites: grain-size and compositional dependence, *Phys. Earth planet. Inter.,* **13,** 260–267.

de Groot, L.V., Dekkers, M.J. & Mullender, T.A.T., 2012. Exploring the potential of acquisition curves of the anhysteretic remanent magnetization as a tool to detect subtle magnetic alteration induced by heating, *Phys. Earth planet. Inter.,* **194–195,** 71–84.

Dekkers, M.J. & Böhnel, H.N., 2006. Reliable absolute palaeointensities independent of magnetic domain state, *Earth planet. Sci. Lett.,* **248,** 508–517.

Dodson, M.H. & McClelland-Brown, E., 1980. Magnetic blocking temperatures of single-domain grains during slow cooling, *J. geophys. Res.,* **85,** 2625–2637.

Dunlop, D.J., 2002. Theory and application of the Day plot (Mrs/ Msversus Hcr/ Hc) 1. Theoretical curves and tests using titanomagnetite data, *J. geophys. Res.,* **107,** doi:10.1029/2001JB000486.

Dunlop, D.J. & Özdemir, Ö., 1997. *Cambridge Studies in Magnetism: Rock Magnetism: Fundamentals and Frontiers,* Cambridge University Press, Cambridge, UK.

Fabian, K. & Leonhardt, R., 2010. Multiple-specimen absolute paleointensity determination: an optimal protocol including pTRM normalization, domain-state correction, and alteration test, *Earth planet. Sci. Lett.,* **297,** 84–94.

Ferk, A., Aulock, F.W.V., Leonhardt, R., Hess, K.U. & Dingwell, D.B., 2010. A cooling rate bias in paleointensity determination from volcanic glass: an experimental demonstration, *J. geophys. Res.,* **115,** doi:10.1029/2009JB006964.

Haag, M., Dunn, J. & Fuller, M., 1995. A new quality check for absolute palaeointensities of the Earth magnetic field, *Geophys. Res. Lett.,* **22,** 3549–3552.

Halgedahl, S., Day, R. & Fuller, M., 1980. The effect of cooling rate on the intensity of weak-field TRM in single-domain magnetite, *J. geophys. Res.,* **85,** 3690–3698.

Harris, A.J. & Rowland, S., 2001. FLOWGO: a kinematic thermo-rheological model for lava flowing in a channel, *Bull. Volcanol.,* **63,** 20–44.

Herrero-Bervera, E. & Valet, J.-P., 2009. Testing determinations of absolute paleointensity from the 1955 and 1960 Hawaiian flows, *Earth planet. Sci. Lett.,* **287,** 420–433.

Hill, M.J. & Shaw, J., 1999. Palaeointensity results for historic lavas from Mt Etna using microwave demagnetization/remagnetization in a modifiedThellier-type experiment, *Geophys. J. Int.,* **139,** 583–590.

Hill, M.J. & Shaw, J., 2000. Magnetic field intensity study of the 1960 Kilauea lava flow, Hawaii, using the microwave palaeointensity technique, *Geophys. J. Int.,* **142,** 487–504.

Hon, K., Kauahikaua, J., Denlinger, R. & Mackay, K., 1994. Emplacement and inflation of pahoehoe sheet flows: observations and measurements of active lava flows on Kilauea Volcano, Hawaii, *Geol. Soc. Am. Bull.,* **106,** 351–370.

Juarez, M., Tauxe, L., Gee, J. & Pick, T., 1998. The intensity of the Earth's magnetic field over the past 160 million years, *Nature,* **394,** 878–881.

Kattenhorn, S.A. & Schaefer, C.J., 2008. Thermal–mechanical modeling of cooling history and fracture development in inflationary basalt lava flows, *J. Volc. Geotherm. Res.,* **170,** 181–197.

Kono, M. & Ueno, N., 1977. Paleointensity determination by a modified Thellier method, *Phys. Earth planet. Inter.,* **13,** 305–314.

Krasa, D., Heunemann, C., Leonhardt, R. & Petersen, N., 2003. Experimental procedure to detect multidomain remanence during Thellier-Thellier experiments, *Phys. Chem. Earth,* **28,** 681–687.

Leonhardt, R., Heunemann, C. & Krasa, D., 2004. Analyzing absolute paleointensity determinations: acceptance criteria and the software Thellier-Tool4.0. Geochem, *Geophys. Geosyst.,* **5,** doi:10.1029/2004GC000807.

Leonhardt, R., Matzka, J., Nichols, A. & Dingwell, D., 2006. Cooling rate correction of paleointensity determination for volcanic glasses by relaxation geospeedometry. *Earth planet. Sci. Lett.,* **243,** 282–292.

McClelland-Brown, E.M.C., 1984. Experiments on TRM intensity dependence on cooling rate, *Geophys. Res. Lett.,* **11,** 205–208.

Mullender, T.A.T., van Velzen, A.J. & Dekkers, M.J., 1993. Continuous drift correction and separate identification of ferromagnetic and paramagnetic contributions in thermomagnetic runs, *Geophys. J. Int.,* **114,** 663–672.

Muxworthy, A.R., 2010. Revisiting a domain-state independent method of palaeointensity determination, *Phys. Earth planet. Inter.,* **179,** 21–31.

Parry, L.G., 1965, Magnetic properties of dispersed magnetite powders, *Philos. Mag.,* **11,** 303–312.

Peck, D.L., 1978. Cooling and Vesiculation of Alae Lava Lake, Hawaii. Geological Survey Professional Paper 935-B, Repeated measurements of temperatures in drill holes and the altitude of the surface document the cooling of a thin ponded basalt flow, pp. 1–65.

Peck, D.L., Hamilton, M.S. & Shaw, H.R., 1977. Numerical analysis of lava lake cooling models; Part II, Application to Alae lava lake, Hawaii, *Am. J. Sci.,* **277,** 415–437.

Perrin, M., 1998. Paleointensity determination, magnetic domain structure, and selection criteria, *J. geophys. Res-Sol Ea,* **103,** 30 591–30 600.

Prévot, M., Lecaille, A. & Mankinen, E.A., 1981. Magnetic effects of maghemitization of oceanic crust, *J. geophys. Res.,* **86,** 4009–4020.

Riisager, P. & Riisager, J., 2001. Detecting multidomain magnetic grains in Thellier palaeointensity experiments, *Phys. Earth planet. Inter.,* **125,** 111–117.

Selkin, P.A. & Tauxe, L., 2000. Long-term variations in palaeointensity, *Philos. T. Roy. Soc. A,* **358,** 1065–1088.

Shaw, H.R., Hamilton, M.S. & Peck, D.L., 1977. Numerical analysis of lava lake cooling models; Part I, Description of the method, *American Journal of Science,* **277,** 384–414.

Tanguy, J.C., 1975. Intensity of the geomagnetic field from recent Italian lavas using a new paleointensity method, *Earth planet. Sci. Lett.,* **27,** 314–320.

Tauxe, L., Pick, T. & Kok, Y., 1995. Relative paleointensity in sediments: a pseudo-Thellier approach, *Geophys. Res. Lett.,* **22,** 2885–2888.

Tauxe, L. & Staudigel, H., 2004. Strength of the geomagnetic field in the Cretaceous Normal Superchron: new data from submarine basaltic glass of the Troodos Ophiolite, *Geochem. Geophys. Geosyst.,* **5,** doi:10.1029/2003GC000635.

Thellier, E. & Thellier, O., 1959. Sur l'intensité du champ magnétique terrestre dans le passé historique et géologique, *Ann. Geophys.,* **15,** 285–378.

Valet, J.P. & Soler, V., 1999. Magnetic anomalies of lava fields in the Canary islands. Possible consequences for paleomagnetic records, *Phys. Earth planet. Inter.,* **115,** 109–118.

Valet, J.P., Tric, E., Herrero-Bervera, E., Meynadier, L. & Lockwood, J.P., 1998. Absolute paleointensity from Hawaiian lavas younger than 35 ka, *Earth planet. Sci. Lett.,* **161,** 19–32.

Walton, D. & Williams, W., 1988. Cooling rate effects in the magnetization of single-domain grains, *J. Geomag. Geoelectr.,* **40,** 729–737.

Wright, T.L. & Okamura, R.T., 1977. Cooling and crystallization of Tholeiitic Basalt, 1965 Makaopuhi Lava Lake, Hawaii. Geological Survey Professional Paper 1004, An account of the 4-year history of cooling, crystallization, and differentiation of tholeiitic basaltfrom one of Kilauea's lava lakes, pp. 1–83.

Yu, Y., 2011. Importance of cooling rate dependence of thermoremanence in paleointensity determination, *J. geophys. Res.,* **116**.

Yu, Y. & Tauxe, L., 2005. Testing the IZZI protocol of geomagnetic field intensity determination, *Geochem. Geophys. Geosyst.,* **6**.

Yu, Y., Tauxe, L. & Genevey, A., 2004. Toward an optimal geomagnetic field intensity determination technique, *Geochem. Geophys. Geosyst.,* **5,** Q02H07, doi:10.1029/2003GC000630.